Original Article

MOLECULAR METABOLISM

FGF21 mimetic antibody stimulates UCP1-independent brown fat thermogenesis via FGFR1/βKlotho complex in non-adipocytes

Mark Z. Chen [1], Joshua C. Chang [1], Jose Zavala-Solorio [1], Lance Kates [1], Minh Thai [1], Annie Ogasawara [2], Xiaobo Bai [1], Sean Flanagan [3], Victor Nunez [3], Khanhky Phamluong [1], James Ziai [3], Robert Newman [1], Søren Warming [1], Ganesh Kolumam [1], Junichiro Sonoda [1,*]

ABSTRACT

Objective: Fibroblast Growth Factor 21 (FGF21) is a potent stimulator of brown fat thermogenesis that improves insulin sensitivity, ameliorates hepatosteatosis, and induces weight loss by engaging the receptor complex comprised of Fibroblast Growth Factor Receptor 1 (FGFR1) and the requisite coreceptor βKlotho. Previously, recombinant antibody proteins that activate the FGFR1/βKlotho complex were proposed to act as an FGF21-mimetic; however, in vivo action of these engineered proteins has not been well studied.

Methods: We investigated the mechanism by which anti-FGFR1/βKlotho bispecific antibody (bFKB1) stimulates thermogenesis in UCP1-expressing brown adipocytes using genetically engineered mice. Anti-FGFR1 agonist antibody was also used to achieve brown adipose tissue restricted activation in transgenic mice.

Results: Studies with global *Ucp1*-deficient mice and adipose-specific *Fgfr1* deficient mice demonstrated that bFKB1 acts on targets distal to adipocytes and indirectly stimulates brown adipose thermogenesis in a UCP1-independent manner. Using a newly developed transgenic system, we also show that brown adipose tissue restricted activation of a transgenic FGFR1 expressed under the control of *Ucp1* promoter does not stimulate energy expenditure. Finally, consistent with its action as a FGF21 mimetic, bFBK1 suppresses intake of saccharin-containing food and alcohol containing water in mice.

Conclusions: Collectively, we propose that FGFR1/βKlotho targeted therapy indeed mimics the action of FGF21 in vivo and stimulates UCP1-independent brown fat thermogenesis through receptors outside of adipocytes and likely in the nervous system.

Keywords FGF21; Therapeutic antibody; Agonist antibody; Thermogenesis; Brown adipose tissue

1. INTRODUCTION

Obesity is recognized as a leading cause for the development of chronic diseases such as type 2 diabetes mellitus, non-alcoholic steatohepatitis (NASH), cardiovascular disease, and various forms of cancer [1–3]. Under the condition of continual excess calorie consumption, white adipose tissues (WAT) accumulate lipids beyond its innate storage capacity leading to low-grade inflammation, endoplasmic reticulum stress, fibrosis, and insulin resistance [4]. In obese individuals, ectopic lipids also accumulate in non-adipose organs such as liver and skeletal muscle, exacerbating hyperinsulinemia and dyslipidemia, the hallmarks of the metabolic syndrome [5–7]. Therapeutic agents that correct energy imbalance and improve insulin sensitivity by promoting energy expenditure (EE) without significant adverse effects may present a novel approach to treating obesity and its comorbidities. The recent re-discovery of functional thermogenic brown adipose tissues (BAT) in adult humans has led to the examination of this metabolic tissue as a potential pharmacological target for the treatment of obesity [8–12]. Similar to WAT, BAT consists mainly of adipocytes; however, unlike WAT, which acts as a repository for energy storage, BAT serves as an endogenous heating element through combustion of macronutrients [13]. The expression of the inner-mitochondrial protein uncoupling protein 1 (UCP1) defines thermogenic brown adipocytes by its ability to dissipate heat by uncoupling proton transport from ATP synthesis [14]. The stimulation of human BAT activity by mild cold exposure correlates with an increase in the whole body resting metabolic rates, indicating a functional significance

[1]Molecular Biology, Genentech Inc., South San Francisco, CA, USA [2]Biomedical Imaging, Genentech Inc., South San Francisco, CA, USA [3]Pathology, Genentech Inc., South San Francisco, CA, USA

*Corresponding author. 1 DNA Way, South San Francisco, CA, 94080, USA. E-mail: junichis@gene.com (J. Sonoda).

Abbreviations: AUC, area under the curve; BAT, brown adipose tissue; ECD, extracellular domain; EE, energy expenditure; eWAT, epididymal white adipose tissue; FDG, fluorodeoxyglucose; FGF21, Fibroblast Growth Factor 21; FGFR1, Fibroblast Growth Factor Receptor 1; HFD, high-fat diet; iBAT, interscapular brown adipose tissue; HMW, high molecular weight; ingWAT, inguinal white adipose tissue; KLB, βKlotho; MAPK, mitogen-activated protein kinase; NASH, non-alcoholic steatohepatitis; UCP1, uncoupling protein 1; WAT, white adipose tissue

Received July 8, 2017 • Revision received September 8, 2017 • Accepted September 12, 2017 • Available online 18 September 2017

http://dx.doi.org/10.1016/j.molmet.2017.09.003

[15]. In adult humans, BAT can be found most prominently in the supraclavicular area but is also found in other regions in the upper body [10,11]. In rodents, BAT can be found throughout the body, but most prominently in the interscapular region (interscapular BAT or iBAT) [16].

Fibroblast Growth Factor 21 (FGF21) is an endocrine member of the FGF super family that has been identified as a regulator of BAT thermogenesis and nutrient metabolism [17,18]. Recombinant FGF21 protein and its modified forms exhibit potent anti-obesity and insulin-sensitizing effects associated with increased BAT thermogenesis in rodents [19,20]. Certain aspects of the anti-obese and insulin sensitizing effects of these molecules have also been observed in non-human primates and humans [21–25]. FGF21 functions as a ligand for the receptor complexes consisting of FGFR and βKlotho (KLB) [26]. While FGF21 is capable of activating three FGFR isoforms (1c, 2c, and 3c) in tandem with KLB [27], FGFR1c appears to play the predominant role in mediating its metabolic effects in obese mice. First, *aP2*-CRE-mediated *Fgfr1* gene deletion almost completely abolishes the metabolic effects of recombinant FGF21 [28,29]. Second, the engineered humanized effector-less bispecific antibody bFKB1 selectively binds and activates the FGFR1/KLB co-receptor complex and largely mimics the action of recombinant FGF21 in mice [30]. In addition, bFKB1 and a different FGFR1/KLB agonist antibody induced weight loss in non-human primates [29,30]. Thus, FGFR1 activation is necessary and sufficient for the metabolic action of FGF21, although FGFR2 and FGFR3 have not yet be ruled out in contributing to the action of FGF21. Both long-acting FGF21 analogs and agonist FGFR1/KLB antibodies have been or are currently being investigated in clinical trials in Type 2 diabetics and obese individuals (e.g., ClinicalTrials.gov, NCT02413372, NCT02538874, NCT02593331, NCT02708576, NCT03060538).

Although pre-clinical and clinical studies suggest that FGF21 analogs or FGFR1/KLB-targeting antibodies may become an effective therapy for obesity related disorders via the ability to improve whole body energy metabolism, the mechanism by which FGFR1/KLB activation leads to BAT thermogenesis remains elusive. Historically the UCP1 protein has been identified as the primary conduit for generating non-shivering thermogenesis through its ability to produce heat from futile cycling [13,14]. Previously, three groups independently tested the activity of FGF21 in *Ucp1* deficient (KO) mice and suggested that the metabolic improvement by FGF21 is independent of UCP1, although the results regarding the requirement of UCP1 in increasing EE showed disagreements [31–33]. Additionally, the tissues that mediate the FGFR1/KLB receptor response are unclear. Much of the early evidence implicated adipose tissue as the central mediator of this effect. The metabolic benefits of FGF21 were absent in lipodystrophic mice [34,35]. Furthermore, it was found that deletion of the *Klb* gene in adipocytes utilizing the *aP2*-CRE system blocks the acute insulin sensitizing effects of FGF21 [36]. Similarly, two independent studies with *aP2*-CRE-mediated *Fgfr1* gene deletion reported the loss of elevated EE and the beneficial metabolic effects associated with the pharmacological administration of FGF21 [28,29]. This conclusion was consistent with the tissue expression pattern of *Fgfr1* and *Klb* mRNA that are co-expressed at high levels in both white and brown adipose tissues [27,37]. Likewise, treatment of cultured primary subcutaneous adipocytes by FGF21 or bFKB1 increases *Ucp1* mRNA expression, supporting the model of direct adipocyte-mediated action [30,38]. At the same time, *Klb* mRNA can also be detected in distinct regions of the brain [39], and selective deletion of the gene in the *Camk2a*-CRE background abolishes the metabolic action of FGF21 [40]. Collectively, these studies suggested that the receptors expressed in adipocytes and specific neurons in the brain are both necessary for the anti-obese and anti-diabetic actions of FGF21.

In the present study, we employ loss-of-function and gain-of-function genetic analyses in mice to address the mechanism and the site of action of FGFR1/KLB agonists using the anti-FGFR1/KLB antibody bFKB1 as a model. We demonstrate that *Ucp1* is not essential for bFKB1 to stimulate BAT thermogenesis in obese mice. Using adipocyte-selective *Fgfr1* gene knockout and a newly developed system to achieve cell-type specific activation of FGFR1 signaling with an agonist antibody, we also find that activation of FGFR1 in brown adipocyte is neither necessary nor sufficient for BAT stimulated EE. Finally, we show that bFKB1, similar to FGF21, alters sweet and alcohol preference, suggesting the role of the nervous system in the action of this antibody. Taken together, our data offers evidence that bFKB1 indeed acts as an FGF21 mimetic protein whose in vivo metabolic activity originates outside of the adipocytes.

2. MATERIALS AND METHODS

2.1. Recombinant proteins

The generation of bFKB1 and 14B6 was described previously [30]. bFKB1 has the human IgG1 backbone with the knob-hole and the effector-attenuating NG modifications. 14B6 has the mouse IgG2a backbone with the effector-attenuating DANG modifications [41]. Recombinant FGFR1 extracellular domain (ECD) proteins were produced either in *E. Coli* or CHO cells and purified using conventional methods.

2.2. Animal studies

All animal studies were conducted in accordance with the Guide for the Care and Use of Laboratory Animals, published by the National Institutes of Health (NIH) (NIH Publication 8523, revised 1985). The Institutional Animal Care and Use Committee (IACUC) at Genentech reviewed and approved all animal protocols. All the mice were maintained in a pathogen-free animal facility under standard 12 h light/12 h dark cycle at 21 °C with access to normal chow (Labdiet 5010) or high-fat diet (HFD; Harlan Teklad TD.06414, 58.4% calories from fat) and water *ad libitum* unless otherwise indicated. All the mice used for intervention studies were around 2–6 months old and were randomized into groups based on body weight, blood glucose levels, and/or specific parameters being examined at the pre-dose state. All antibody doses administered were at a concentration of 10 mg/kg and delivered via intraperitoneal injection.

2.3. Mouse strains

Ucp1 KO mice in C57BL/6J background [42] or the control wild type (WT) mice were bred at The Jackson Laboratory and housed at 30 °C throughout the study after transferring to the Genentech mouse facility. Adipose-specific *Fgfr1* CKO mice were generated by crossing the exon 4 floxed *Fgfr1* CKO mice [43] with *Adipoq*-CRE mice [44,45], both obtained from The Jackson Laboratory. To generate *Ucp1-hmFGFR1c* transgenic mice, a plasmid encoding chimeric FGFR1c (D1 domain from human FGFR1 and the rest from mouse FGFR1) was constructed, linearized, and used for pronuclear injection. This chimeric construct contains 8.4 kb mouse *Ucp1* upstream sequence, a human/mouse chimeric cDNA followed by an SV40 pA signal and 4.3 kb downstream *Ucp1* genomic region (mouse exons 3–6) [46]. A line that selectively expresses *hmFGFR1c* in iBAT was selected by qPCR using human *FGFR1* specific primers (5′-aaccaaaccccgtagctccatat-3′ and 5′-gtcccactggaagggcat-3′).

2.4. Metabolic measurements

Oxymax system (Columbus Instruments) was used to measure oxygen consumption (VO2) and carbon dioxide production (VCO2). After acclimatization to the cages, mice were randomized into groups based on body weight and baseline metabolic parameters. The following equations were used to calculate EE and the respiratory quotient (RQ). $EE = VO2 \times (3.815 + 1.232 \times RQ)$. $RQ = VO2/VCO2$. For core body temperature monitoring, TA-F10 transmitter (DSI) was surgically implanted into the peritoneal cavity. Core body temperature was monitored real-time using DSI Implantable Telemetry System. For GTT, mice were fasted 6 h and given an intraperitoneal (i.p.) injection of 2 g/kg glucose solution. For ^{18}F-FDG uptake measurement, mice were fasted overnight, and, on the next day, approximately 50 μCi ^{18}F-FDG was injected intravenously via the lateral tail vein. Mice were kept warm on a heating pad and euthanized after 1 h of tracer administration. Tissues were harvested and weighed, and radioactivity was measured using a CRC-15W dose calibrator (Capintec) with background subtraction and decay correction against dosing solution standards.

2.5. Sweet taste and alcohol preference

Taste preference studies were performed using AIN-93G-based diets with or without 0.2 % wt/v saccharin (#240931, Sigma–Aldrich) (TD.150849 and TD.120590, respectively, Envigo). Single housed mice were given the control diet for 14 days and then an equal access to both diets and water *ad libitum* for another 14 days. Food intake was measured every 2 or 3 days, and food positions were switched randomly throughout the study. Alcohol preference studies were performed using a two-bottle system containing vivarium water or diluted ethanol with vivarium water. Animals were singly housed and acclimated sequentially on increasing amounts of ethanol for 7 days per concentration. After 10 days of acclimation on desired ethanol concentration, animals were randomized based on % alcohol-water consumption and body weight. Fluid consumption was measured every 2 or 3 days and bottle positions were switched randomly throughout the study.

2.6. Gene expression analysis

RNA was isolated by combining Trizol (Life Technologies) RNA separation and column based RNeasy extraction (Qiagen) and used to synthesize cDNA using ABI High Capacity Reverse Transcription kit (ABI) [47]. For qPCR, samples were run in triplicate in the ViiA 7 Real-Time PCR instrument (ABI) using Sybr green dye or TaqMan probes. Primers sequences are available upon request. For each sample, mRNA abundance was normalized by 36B4 or TBP1 house keeping gene expression.

2.7. Histology

Adipose tissues were fixed in 10% formalin for 24 h, and embedded in paraffin before sectioned at 7 μm. Sections were stained with hematoxylin and eosin (H&E), pERK1/2 (Thr202/Tyr204) immunohistochemistry with rabbit monoclonal antibody 20G11 (#4370, Cell Signaling Technologies), or immunofluorescence with rabbit polyclonal to UCP1 (ab23841, Abcam) and DAPI (#62247, Thermo Scientific). Fluorescence images were visualized with LEICA SPE confocal microscope and quantified by ImageJ software.

2.8. In vitro assays

Cell extracts from transiently transfected 293T cells were generated by lysing cells in 2 × LDS buffer (Invitrogen) containing protease and phosphatase inhibitor tablets (Roche). Samples were then sonicated and used for western blot analysis by standard methods. Antibodies used for western blot analysis were generated in house. For luciferase assay, engineered HEK293 cells with CRISPR/Cas9-mediated *FGFR1* gene deletion [30] were transiently transfected with expression vectors encoding appropriate receptors under the CMV promoter, Renilla luciferase (pRL-SV40, Promega), GAL-ELK1 transcriptional activator fusion (pFA2-ELK1, Agilent), and a firefly luciferase reporter driven by GAL4 binding sites (pFR-luc, Agilent), using FuGENE HD Transfection Reagent (Promega). On the next day, the transfected cells were cultured for an additional 6–8 h in serum free DMEM-based media containing an appropriate agonist antibody at various concentrations. The cellular luciferase activity was determined using Dual-Glo Luciferase Assay System (Promega) and EnVision Multilabel Reader (PerkinElmer). Firefly luciferase activity was normalized to the co-expressed Renilla luciferase activity to calculate relative light unit and data presented as fold induction.

2.9. Statistics

Unpaired student's t-test (two-tailed) or one-way ANOVA with post hoc Dunnett's test was used for statistical analysis to compare treatment groups. For energy expenditure and core body temperature results, the mean value was calculated for each mouse for each of the indicated durations, and the values were used to calculate statistical significance between groups. A p-value < 0.05 was considered statistically significant. "ns" stands for no significance. All the values were presented as means ± SEM unless otherwise noted.

3. RESULTS

3.1. bFKB1 enhanced EE and improved metabolic health in the absence of UCP1

To investigate if UCP1 is required for bFKB1 dependent stimulation of EE, *Ucp1* KO and control WT mice on HFD injected with bFKB1 were monitored by indirect calorimetry to measure EE. *Ucp1* KO mice have been reported to be defective in adaptive thermogenesis [42,48,49]. Therefore, both *Ucp1* KO and WT control mice were housed at a thermoneutral temperature (30 °C) throughout the acclimation and experimental period. A single dose of bFKB1 significantly increased EE in WT mice as previously reported [30] (Figure 1A and B). bFKB1 also significantly increased EE in *Ucp1* KO mice, however to a lesser degree (Figure 1A and B). In addition, bFKB1 induced several beneficial effects previously observed in both *Ucp1* KO and WT mice, including lowering of body weight (Figure 1C), serum insulin, triglycerides, and cholesterol (Figure 1D). However, an increase in high molecular weight (HMW) adiponectin and an improvement in glucose tolerance reached significance only in WT mice. To test whether the observed increase in EE in HFD-fed mice is associated with increased thermogenesis, core body temperature was monitored real-time by implanting a telemetry transmitter in the peritoneal cavity. bFKB1 treatment elevated the resting core body temperature in both the WT and *Ucp1* KO groups compared to control IgG (Figure 1E and F), suggesting that UCP1 is dispensable for bFKB1-induced thermogenesis.

3.2. bFKB1 stimulated iBAT nutrient metabolism in the absence of UCP1

Previously, FGF21 and bFKB1 have been shown to increase ^{18}F-fluorodeoxyglucose (^{18}FDG) uptake into iBAT during fasting indicating insulin-independent iBAT stimulation [30,50]. To test if the activity of bFKB1 is *Ucp1*-dependent, a similar experiment was conducted in *Ucp1* KO and WT control mice fasted overnight. As previously reported, bFKB1 injection increased ^{18}FDG uptake into iBAT in WT mice and,

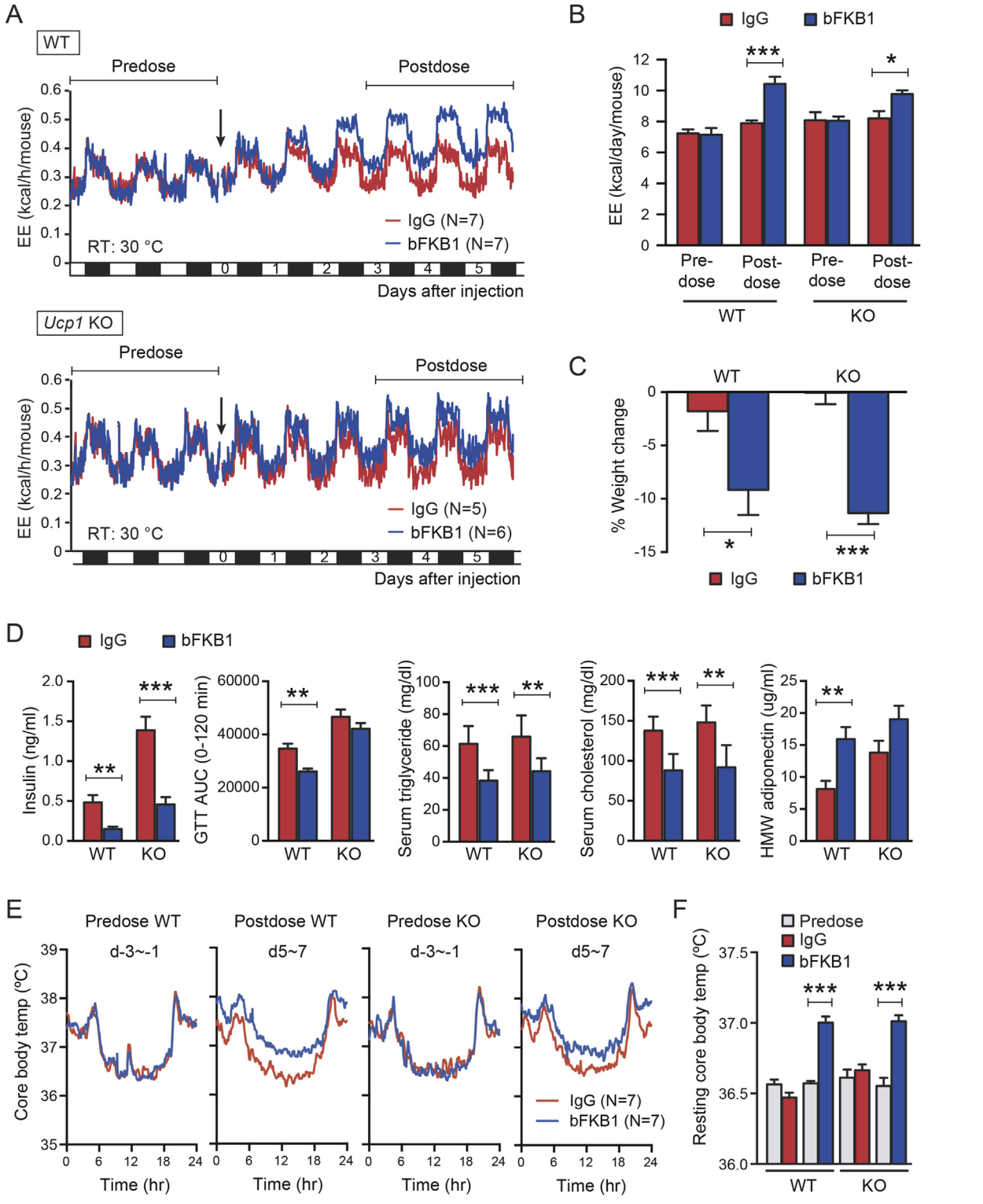

Figure 1: bFKB1 enhances thermogenesis and induces weight loss in HFD-fed *Ucp1* KO mice. (A) Mean EE values in HFD-fed control WT and *Ucp1* KO mice that received single i.p. injection (arrow) at 10 mpk IgG. Mice were maintained at thermoneutrality (30 °C) and were on HFD for 6 weeks at the time of dosing. **(B)** Mean daily EE value ± SEM in indirect calorimetry shown in (A) during the indicated pre- and post-dose periods. **(C)** Average % body weight change after 5 days of exposure to bFKB1. The pre-dose body weights were 31.9 ± 0.8 g (WT) and 38.6 ± 1.3 g (KO). **(D)** Area under the blood glucose curve (AUC) in GTT and serum parameters on 14 days post injection. **(E)** Mean core body temperature as measured by intraperitoneally implanted telemetry transponder in mice receiving a single i.p. injection of bFKB1 or control IgG at 10 mpk. Mice were maintained at thermoneutrality (30 °C) and were on HFD for 8 weeks at the time of dosing. The data shown are the mean values within 48-h period before and after dosing. **(F)** Mean body temperature between 6 AM and 6 PM (i.e. resting period) during the pre-dose and post-dose periods indicated in (E). In (A) and (E), error bars omitted for clarity. Other data are mean ± SEM. $p < 0.05$ (*), <0.01 (**), <0.001 (***) vs control.

unexpectedly, more so in *Ucp1* KO mice (Figure 2A). ^{18}FDG uptake did not change significantly in any other tissues measured including pancreas, liver, inguinal WAT (ingWAT), and epididymal WAT (eWAT) (Figure 2A). bFKB1 treatment also decreased the size of lipid droplets and increased the nuclear density in iBAT in WT mice (Figure 2B and C). These changes occur to a greater extent in the *Ucp1* KO mice, suggesting more efficient depletion of lipid droplets and overall lowered cell volume, perhaps due to an enhanced substrate demand and utilization in the KO mice (Figure 2B and C). UCP1 protein expression as detected by immunofluorescence was elevated in WT mice treated with bFKB1 and was expectedly absent in the KO mice (Figure 2B).

3.3. bFKB1 stimulated EE independent of FGFR1 in adipocytes

To further dissect the mechanism by which bFKB1 stimulates BAT thermogenesis, we generated mice bearing a floxed *Fgfr1* allele and adipocyte-selective CRE driver, *Adiponectin* (*Adipoq*)-CRE to generate adipose-specific *Fgfr1* deficient (*Fgfr1*^{Adipoq} CKO) mice [43–45] (Supplementary Fig. S1). Mice with homozygous floxed *Fgfr1* allele

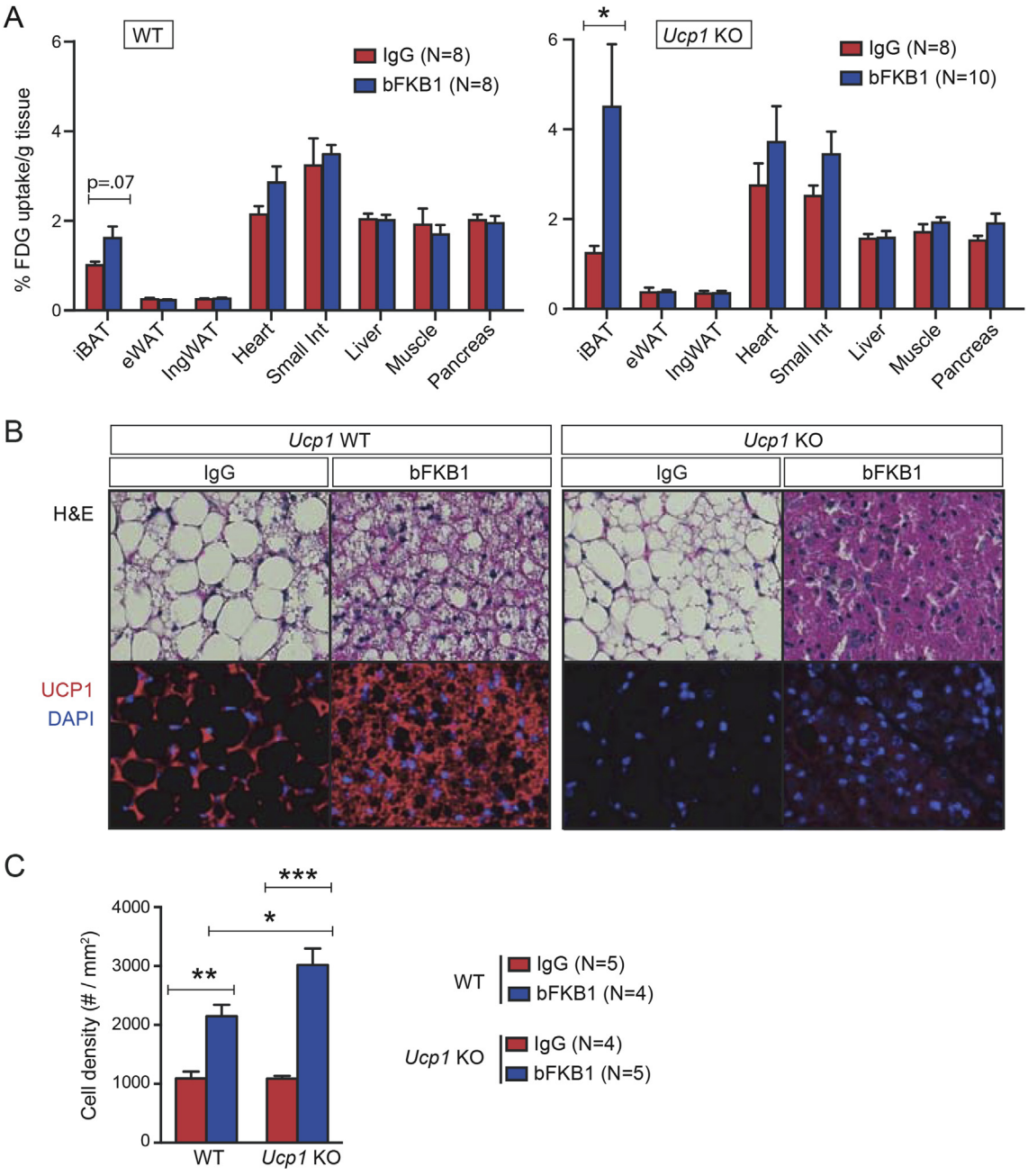

Figure 2: bFKB1 stimulates iBAT activity in *Ucp1* KO mice on HFD. (A) Tissue FDG-uptake in control WT and *Ucp1* KO mice at 5 days after single i.p. injection of indicated IgG at 10 mpk. Mice were fasted overnight before FDG-uptake measurement. Data are mean ± SEM and represent % of dose given, normalized by tissue weight. Mice on HFD were maintained at thermoneutrality (30 °C). **(B)** H&E staining (top) and anti-UCP1 and DAPI staining of iBAT sections from WT or *Ucp1* KO mice on HFD for 5 weeks, after 7 days of treatment with IgG or bFKB1 at 10 mpk. Representative sections are shown. **(C)** Quantification of cell density on the basis of the number of DAPI-positive nuclei per area in iBAT tissue sections. Error bars are ± SEM. $p < 0.05$ (*), <0.01 (**), <0.001 (***) vs control.

but without *Adipoq*-CRE driver (*Fgfr1*$^{fl/fl}$) were used as a control. At baseline, *Fgfr1* mRNA levels in brown and white adipose tissues, but not in the kidney, were decreased in *Fgfr1*^{Adipoq} CKO mice as anticipated (Figure 3A). No consistent changes were observed in the proximal targets of FGFR1 signaling pathways, *Spread1*, *Dusp6*, or *Spry4* [40,51,52], suggesting that adipocyte FGFR1 is not constitutively activated at the baseline. Both of the genetically engineered alleles used here have been previously validated for generation of cell-type specific gene deletion; however, a residual level of *Fgfr1* mRNA expression was detectable by qPCR in *Fgfr1*^{Adipoq} CKO mice (Figure 3A). This is likely because *Fgfr1* mRNA, unlike *Klb* mRNA, is abundantly expressed in stromal cells within white and brown adipose tissues, such as endothelial cells, preadipogenic fibroblasts, and infiltrating immune cells [53–55]. To assess the extent of the *Fgfr1*

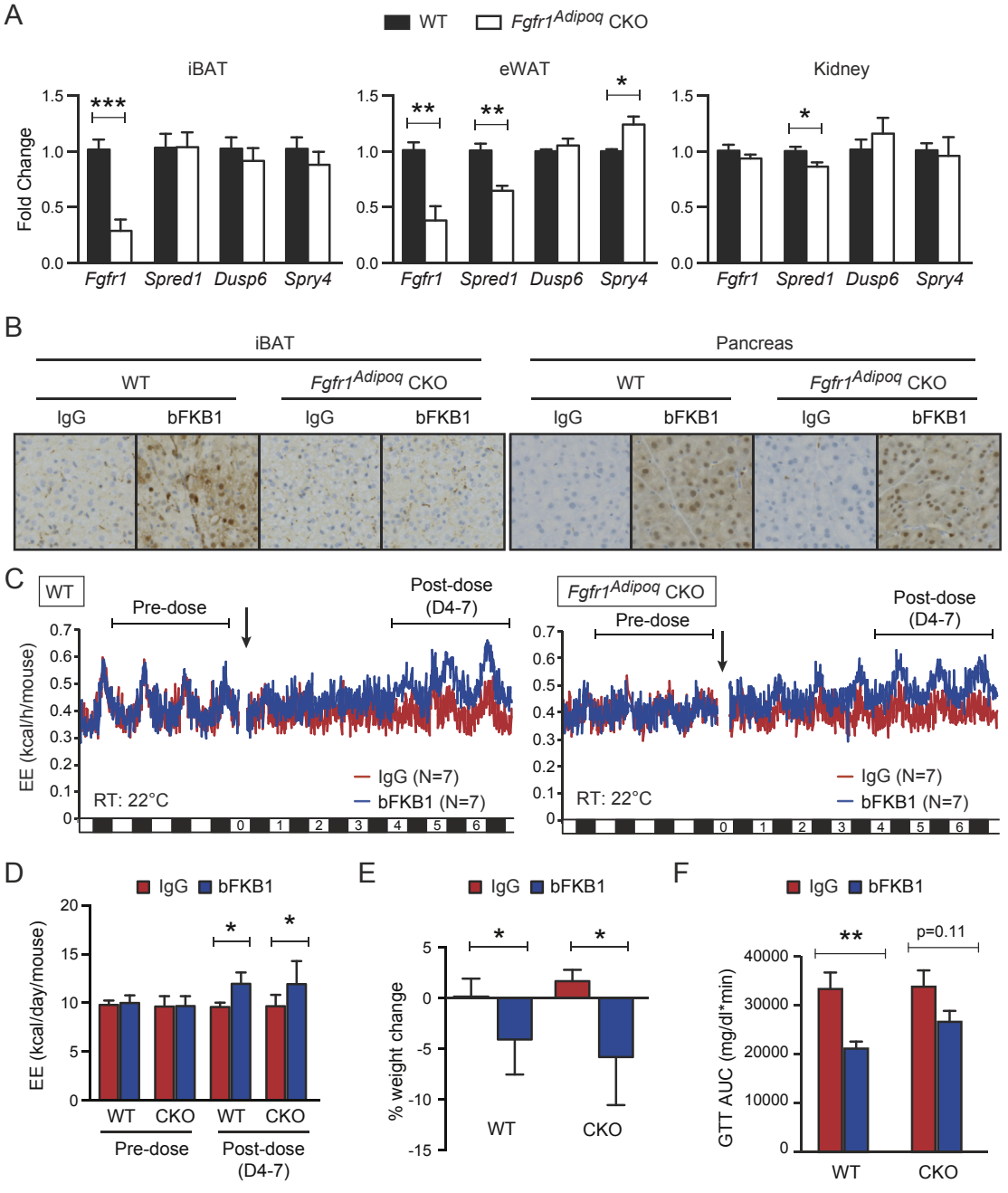

Figure 3: bFKB1 stimulates EE in adipose-selective *Fgfr1* CKO mice on normal chow. (A) Tissue mRNA expression at baseline normalized to WT animals. N = 4–5 mice per group. **(B)** Induction of ERK phosphorylation by bFKB1 in iBAT and pancreas in control WT and *Fgfr1*^{Adipoq} CKO mice. Tissues were harvested 1 h after i.p. injection of indicated antibody at 10 mg/kg, and subjected to immunohistochemistry using antibody specific to phosphorylated ERK. 4–5 mice per group were examined and representative images are shown for each group. **(C)** Mean EE values in control WT and *Fgfr1*^{Adipoq} CKO mice receiving single 10 mg/kg dose of antibody. **(D)** Mean daily EE value ± SEM in indirect calorimetry shown in (A) during the indicated pre- and post-dose periods. **(E)** Average % body weight change after 5 days of exposure to bFKB1. The pre-dose body weights were 28.4 ± 1.9 g (WT) and 28.4 ± 2.4 g (CKO). **(F)** Area under the blood glucose curve (AUC) during GTT. In (C), error bars omitted for clarity. Other data are mean ± SEM. $p < 0.05$ (*), <0.01 (**), <0.001 (***) vs control.

gene deletion with spatial and functional information, we sought to determine the loss of FGFR1 function by monitoring bFKB1-induced MAPK signal activation using immunohistochemistry. Mice were given an acute i.p. dose of bFKB1 and tissues were collected for histology after 1 h. The degree of MAPK signaling activation was assessed by staining tissue slices with an anti-phosphorylated ERK (pERK) antibody as an indicator of FGFR1/KLB receptor engagement. An increased level of pERK staining was detected in both the iBAT and pancreatic acinar cells in the control *Fgfr1*$^{fl/fl}$ mice administered with bFKB1 (Figure 3B and Supplementary Fig. S2). bFKB1 also increased pERK staining in the pancreatic acinar cells in *Fgfr1*^{Adipoq} CKO mice but not in iBAT, indicating a functional loss of adipocyte FGFR1 in *Fgfr1*^{Adipoq} CKO mice.

Next, the metabolic action of bFKB1 in chow-fed *Fgfr1*^{Adipoq} CKO mice was examined by using indirect calorimetry. As shown in Figure 3C and D, a single injection of bFKB1 caused a gradual increase in EE in both *Fgfr1*^{Adipoq} CKO and the control *Fgfr1*$^{fl/fl}$ mice (Figure 3C and D). Additionally, body weight significantly decreased in both groups treated with bFKB1 (Figure 3E). On day 9 post dose, *Fgfr1*$^{fl/fl}$ mice treated with bFKB1 showed reduced glucose excursion during GTT as measured by the difference in area under the curve (AUC). In *Fgfr1*^{Adipoq} CKO mice, the glucose excursion trended downwards but did not reach statistical significance (Figure 3F).

The effect of bFKB1 was further assessed in metabolically deranged HFD-fed mice. To eliminate the possibility of temperature induced BAT expansion influencing the results, both *Fgfr1*^{Adipoq} CKO and the control *Fgfr1*$^{fl/fl}$ mice were housed in thermoneutrality (30 °C) throughout the duration of the study. Similar to the normal chow cohort, bFKB1 increased EE in both in *Fgfr1*^{Adipoq} CKO and the control *Fgfr1*$^{fl/fl}$ mice on HFD (Figure 4A and B). bFKB1 also induced significant weight loss in *Fgfr1*^{Adipoq} CKO mice while the weight loss in *Fgfr1*$^{fl/fl}$ mice did not reach significance (Figure 4C). On day 9 after antibody treatment, glucose excursion during GTT was reduced in both WT and KO animals treated with bFKB1, although AUC did not reach significance in either strain (Figure 4D). Serum insulin, cholesterol and fasted glucose levels were significantly reduced in both *Fgfr1*^{Adipoq} CKO and the control *Fgfr1*$^{fl/fl}$ mice; however, free fatty acids and HMW adiponectin reached significance only in the *Fgfr1*$^{fl/fl}$ mice (Figure 4E). To verify the loss of FGFR1 activity in *Fgfr1*^{Adipoq} CKO mice, FGF21 responsive genes in BAT were evaluated by qPCR (Figure 4F). As anticipated, bFKB1 induced *Spred1*, *Dusp6*, *Spry4* expression in *Fgfr1*$^{fl/fl}$ mice, but not in *Fgfr1*^{Adipoq} CKO mice, consistent with the functional loss of FGFR1 in *Fgfr1*^{Adipoq} CKO mice. An increased expression of BAT signature genes, *Ucp1* and *Dio2*, was observed in *Fgfr1*$^{fl/fl}$ mice, but not in *Fgfr1*^{Adipoq} CKO mice. Unexpectedly, the expression of *Spred1*, *Dusp6*, *Spry4*, and *Dio2*, were increased at baseline in *Fgfr1*^{Adipoq} CKO mice with their levels in this condition reaching those observed in bFKB1-treated wild type mice (Figure 4F). This may represent a compensatory signaling event that is metabolically inconsequential. Finally, expression of *Fgfr1* mRNA was reduced in *Fgfr1*^{Adipoq} CKO mice as anticipated. Collectively, lack of FGFR1 signaling at *Adipoq*-CRE expressing adipocytes does not eliminate the bFKB1 induced increase in EE or improved glucose tolerance in either chow-fed or HFD-fed mice, although some aspects of bFKB1 activity appeared to be somewhat compromised.

3.4. Targeted activation of FGFR1 in UCP1-expressing brown adipocytes is not sufficient for enhancement of EE

Even if FGFR1 expressed in adipocytes is not necessary for the metabolic action of FGFR1/KLB agonists, it is formally possible that FGFR1 expressed in adipocytes and somewhere else (e.g., brain) plays a redundant role. Thus, we wanted to test if the activation of FGFR1 in brown adipocytes leads to stimulation of BAT thermogenesis. Our approach was based on a fortuitous discovery of a human-selective anti-FGFR1 agonist monoclonal antibody called 14B6, as described below. The *Fgfr1* gene encodes a single-pass transmembrane protein with three Ig-like domains (D1, D2, and D3) in the ECD (Figure 5A), and is highly conserved among mammalian species. Between mouse and human FGFR1, there are six amino acid differences in D1, 100% identity in D2-D3, and >99% amino acid identity in the cytoplasmic domain. In screening for an FGFR1 agonist, the monoclonal antibody 14B6 mAb was identified as having human FGFR1 specificity while lacking mouse FGFR1 binding. 14B6 mAb detected human FGFR1 but not the mouse ortholog by western blot (Figure 5B). Unsurprisingly, the epitope for 14B6 mAb was mapped by western blot and ELISA to the divergent domain, D1 within ECD, rather than the ligand-binding D2 or D3 domains (Figure 5B and C). In cell-based GAL-ELK1 luciferase assay in engineered HEK293 cells lacking endogenous FGFR1, 14B6 mAb activated human FGFR1, but not mouse FGFR1, when the respective isoforms were exogenously expressed (Figure 5D). In contrast, bFKB1 activated both human and mouse FGFR1 in the presence of KLB as previously demonstrated (Figure 5D) [30].

Based on the strict species specificity of 14B6 mAb, we recognized that it could serve as a useful tool to activate FGFR1 in tissue specific manner in human FGFR1-expressing transgenic mice. To test this idea, a transgenic mouse strain expressing a chimeric human-mouse *FGFR1*/*Fgfr1* gene (c-isoform) under the control of the 8.4 kb mouse *Ucp1* promoter [46] was engineered (Figure 6A). The transgene encodes a chimeric FGFR1c protein consisting of the human D1 domain and the rest of the FGFR1 protein derived from mouse. As anticipated, the transgenic RNA was readily detectable in iBAT tissue but not in other tissues examined in the transgenic *Ucp1-hmFGFR1c* mice (Figure 6B). To validate the in vivo capability of 14B6 mAb to activate the FGFR1 pathway in transgenic *Ucp1-hmFGFR1c* mice, gene expression changes in iBAT were examined in mice that received a single i.p. injection of recombinant effector-less 14B6 mAb or control IgG after 12 days. Consistent with the agonistic activity of 14B6 mAb, expression of FGFR1 regulated genes *Spred1*, *Dusp6*, and *Spry4* was significantly increased in iBAT but not in eWAT (Figure 6C). *Ucp1* did not change in either depot. Despite the ability of 14B6 mAb to activate FGFR1 signaling in the iBAT of transgenic mice, 14B6 mAb failed to enhance EE (Figure 6D and E). Consistent with EE being unaffected, weight change was not different between the two treatment groups (Figure 6F). Moreover, both serum HMW adiponectin and glucose excursion during GTT were unaffected by 14B6 mAb administration in transgenic mice (Figure 6G and H). These series of the gain-of-function experiment indicate that FGFR1 activation in this restricted population of cells is not sufficient to alter EE or glucose tolerance. Given this and the loss-of-function experiment with *Fgfr1*^{Adipoq} CKO mice, we believe that bFKB1 affects BAT metabolism indirectly via a signal originating outside of adipocytes.

3.5. bFKB1 alters sweet food and alcohol preference

The ability of bFKB1 to enhance EE independent of adipocyte FGFR1 and the inability of 14B6 mAb to alter EE while activating FGFR1 in *Ucp1* expressing brown adipocytes indicate an alternative route of action. Recently, two independent studies found that systemic FGF21 administration reduces sweet and alcohol preference in mice by acting directly on the nervous system [56,57]. In particular, von Holstein-Rathlou et al. demonstrated that KLB expressed in the paraventricular nucleus of the hypothalamus regulates taste preference [57]. We asked if specific activation of the FGFR1/KLB complex by bFKB1 mimics these behavioral modifications. To test sweet taste preference, mice were

MOLECULAR METABOLISM

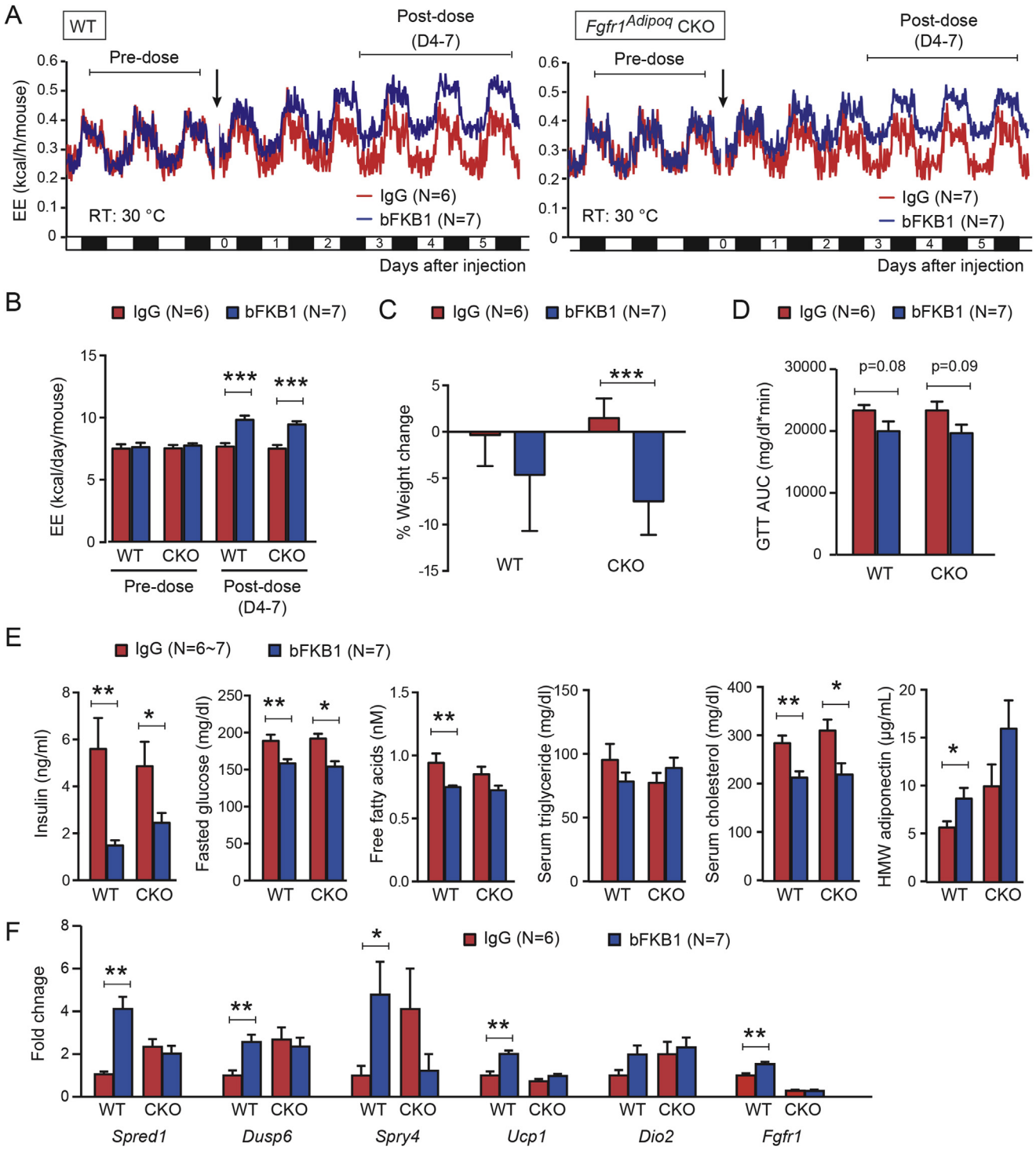

Figure 4: bFKB1 stimulates EE in adipose-selective *Fgfr1* CKO mice on HFD. (A) Mean EE values in control WT and *Fgfr1*^{Adipoq} CKO mice receiving a single 10 mg/kg dose of indicated IgG (Arrow). Mice were maintained at thermoneutrality (30 °C) and were on HFD for 8 weeks at the time of dosing. **(B)** Mean daily EE value ± SEM in indirect calorimetry shown in (A) during the indicated pre- and post-dose periods. **(C)** Average % body weight change after 7 days of exposure to bFKB1. The pre-dose body weights were 45.1 ± 6.0 g (IgG) and 45.5 ± 4.5 g (bFKB1) for WT. For CKO mice, pre-dose weights were 44.9 ± 4.0 (IgG) and 44.8 ± 5.0 (bFKB1). **(D)** AUC in GTT performed on 9 days post-injection. **(E)** Serum parameters on day 11 after IgG or bFKB1 treatment. **(F)** Gene expression changes in BAT measured by qPCR. N = 6–7 mice per group. Gene expression normalized to IgG treated WT animals. In (A), error bars omitted for clarity. Other data are mean ± SEM. $p < 0.05$ (*), <0.01 (**), <0.001 (***) vs control.

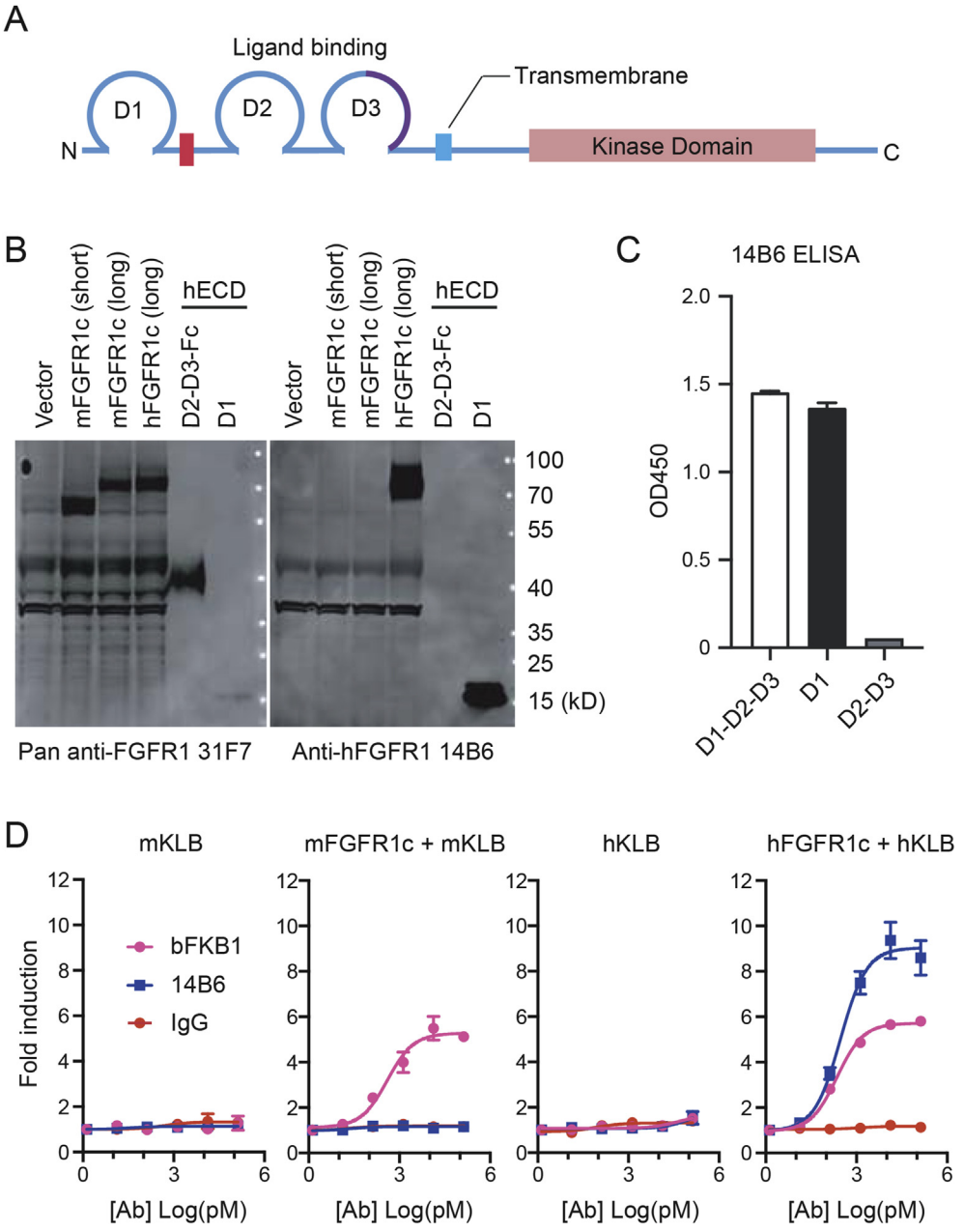

Figure 5: Discovery of human-specific FGFR1 agonist 14B6 mAb. (A) Topological organization of FGFR1 protein. ECD consists of D1, D2, and D3, the acidic box (red). The alternatively spliced region in D3 that differs between "b" and "c" isoforms is indicated in purple. **(B)** Transfected 293T cell lysate (lane 1–4) and purified D1, D2-D3 recombinant protein (lane 5–6) were run on SDS-PAGE and subjected to western blot analysis with a pan-FGFR1 antibody 31F7 that detects both mouse and human FGFR1 through binding to D2-3 domains (left) or with the human specific FGFR1 antibody 14B6 that binds to human but not mouse D1 domain (right). **(C)** ELISA to detect purified protein domains of hFGFR1c by anti-hFGFR1 14B6. **(D)** GAL-ELK1 luciferase assay in engineered HEK293 cell line lacking *FGFR1* gene. Cells were transfected to express indicated receptor and the appropriate reporter construct. Various concentrations of bFKB1 and 14B6 antibodies were tested for agonistic activity. Mean fold induction ± SEM was plotted.

given equal access to unsweetened control chow and chow sweetened with the nonnutritive sweetener saccharin. After 7 days of acclimation with both diets bFKB1 was dosed on day 0 and again at day 18. As expected, bFKB1 significantly lowered body weight compared to the IgG treated group (Figure 7A). While losing weight, the bFKB1 treatment arm increased their total accumulated food intake (Figure 7B). At the same time, bFKB1 decreased the ratio of saccharin diet consumed per day compared to the IgG treated group (Figure 7C).

To examine if bFKB1 impels a change to alcohol preference, mice were given access to ethanol containing water and regular water in a two-bottle system (Figure 7D). Two different alcohol concentrations were tested, 4% and 12%. Animals were acclimated to their respective alcohol concentrations for 10 days before dosing. bFKB1 did not appreciably lower the mouse's predilection for 4% alcohol. Mice adapted to 12% ethanol, on the other hand, exhibited a gradual and significant lowering of the percentage of alcohol containing water

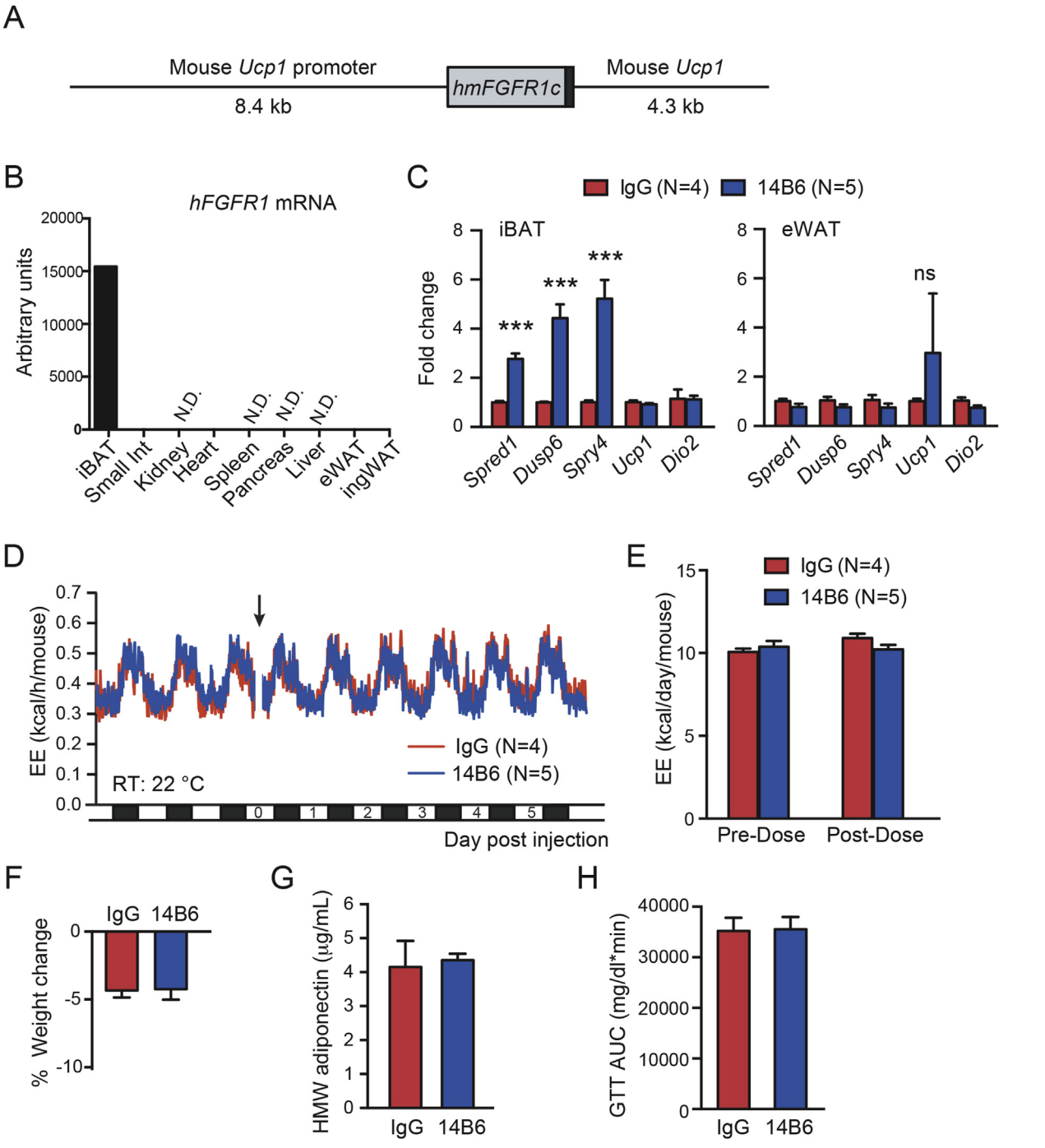

Figure 6: BAT-restricted activation of hFGFR1c transgene by human specific FGFR1 agonist does not stimulate EE. (A) Schematic representation of chimeric *Ucp1-hmFGFR1c* transgenic construct. **(B)** Tissue expression pattern of the transgene assessed by qPCR. **(C)** Gene expression in iBAT and eWAT of *Ucp1-hmFGFR1c* transgenic mice treated with control IgG or 14B6 at 10 mg/kg, assessed by qPCR. **(D)** Mean EE values from hFGFR1 transgenic mice treated with control IgG or 14B6, 10 mg/kg. **(E)** Quantification of the data shown in (D). Average EE per day per mouse pre- and post-doses are shown. **(F)** Average % body weight change 8 days post injection. **(G)** Serum HMW adiponectin 12 days after dose. **(H)** Area under the blood glucose curve during GTT in *Ucp1-hmFGFR1c* transgenic mice. In (D), error bars omitted for clarity. Error bars are mean ± SEM. $p < 0.001$ (***) vs control.

consumed upon a single bFKB1 administration. The weight of both cohorts of animals consuming the different ethanol concentrations was significantly decreased (Figure 7E). Overall, these data show that bFKB1 functions similar to the hormone FGF21 in altering sweet food and alcohol preference, likely via the nervous system.

4. DISCUSSION

Clinical trials with modified human FGF21 analogs LY2405319 and PF05231023 have demonstrated remarkable metabolic effects in obese and diabetic human subjects [21,24]. Identification of the FGFR1/

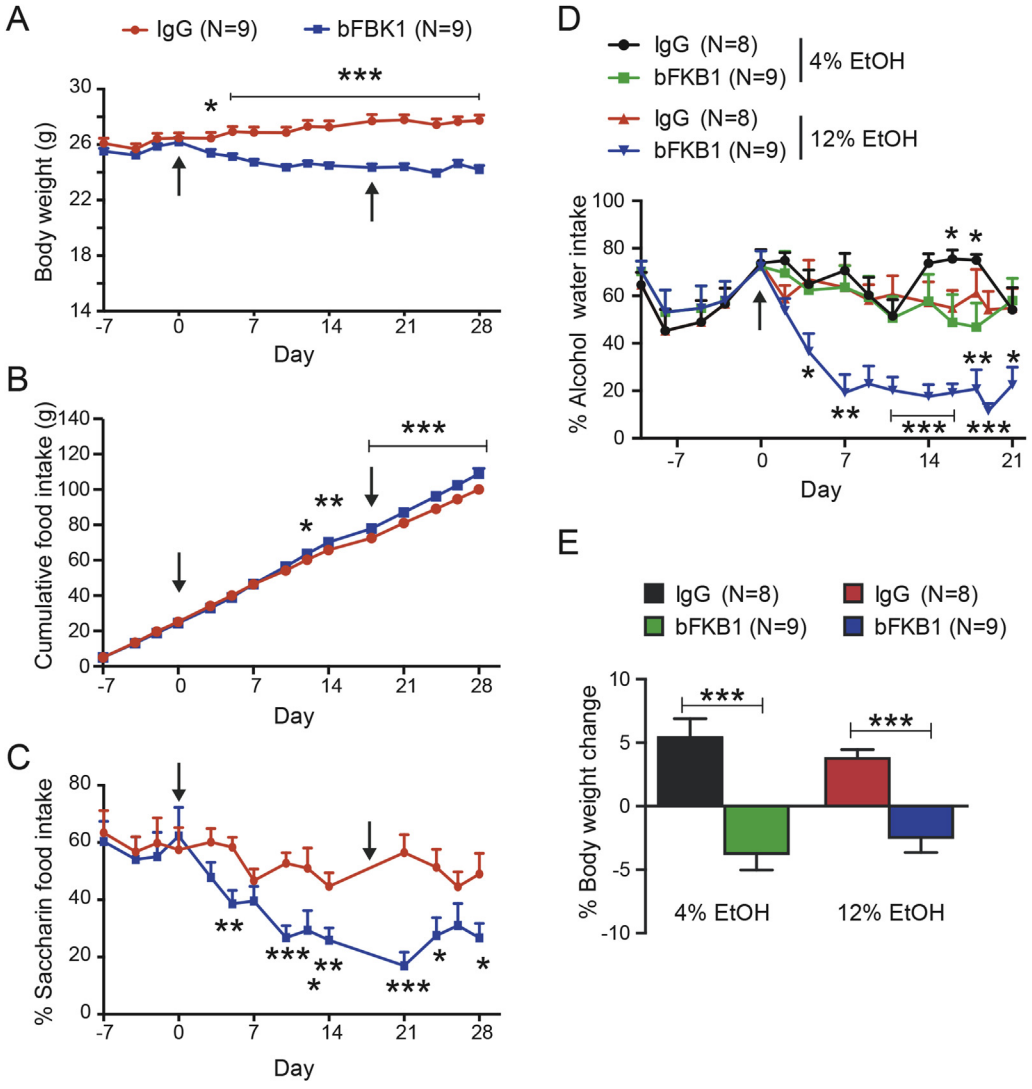

Figure 7: bFKB1 reduces sweet-food and alcohol preference. (A) Body weight, **(B)** total food consumption, and **(C)** % Saccharin-containing food consumption pre- and post-antibody injection. Mice were given access to both control chow and saccharin-containing chow. The indicated antibody was administered on day 0 and 17 at 10 mg/kg each time (arrows). **(D)** % Alcohol-containing water consumption pre- and post-antibody injection. Mice were given access to two water bottles, one containing regular water and the other containing 4 or 12% ethanol in water. After acclimation to alcohol, mice were injected with 10 mg/kg of the indicated antibody on day 0 (arrow). **(E)** % body weight change between IgG vs bFKB1 treated mice in the alcohol preference study on day 21. Data are mean ± SEM. $p < 0.05$ (*), <0.01 (**), <0.001 (***) vs control.

KLB receptor complex as the functional target for FGF21 enabled the generation of agonist antibodies that specifically activate this complex such as BFKB8488A and NGM313, which are also under clinical investigation (ClinicalTrials.gov, NCT02593331, NCT02708576, and NCT03060538). These therapeutic antibodies are designed to function similar to FGF21; however, unlike FGF21, they bypass activation of FGFR2 or 3 in complex with KLB. Each molecule could also show distinct affinity and binding epitope, leading to unique biological activities, as we have recently reviewed [58]. The bispecific anti-FGFR1/KLB agonist antibody bFKB1 acts on the mouse receptor complex and therefore provides a unique opportunity to investigate the mechanisms by which a long-acting FGF21 mimetic antibody affects animal physiology [30]. In this study, the action of bFKB1 and FGF21 were not directly compared due to the vastly different pharmacokinetic profiles of the respective molecules. Nevertheless, by comparing with what has been described with FGF21, the findings presented here corroborate the assumption that bFKB1 indeed behaves like previously studied recombinant FGF21 analogs in vivo, defining it as a long-acting FGF21-mimetic antibody. Our new data also clarify some of the disagreements from previous studies with FGF21 analogs regarding the mechanism of action downstream of the FGFR/KLB complex activation.

UCP1 has traditionally been thought to be indispensable for adaptive thermogenesis in BAT [48,59]. Recently, two independent groups used *Ucp1* KO mice to test the requirement of this gene in the enhancement of EE by human FGF21 or stabilized Fc-FGF21 fusion protein [31,32]. Véniant et al. observed that FGF21 increased EE in both heterozygous and *Ucp1* KO mice. In contrast, Samms et al. reported that continuous FGF21 infusion led to a gradual increase in EE in WT mice; however, this change was absent in *Ucp1* KO mice. The reason for this discrepancy is not clear. However, one possibility could be due to the difference in the housing temperature for each experiment (30 °C in Véniant et al., and slightly lower 26 °C in Samms et al.). In order to avoid the secondary defects associated with *Ucp1* deficiency [49], we conducted our experiment at 30 °C with bFKB1 with *Ucp1* KO mice and control WT mice. The results were consistent with Véniant et al., in that FGFR1/KLB activation leads to an apparent elevation in EE even in *Ucp1*

KO mice, although the effect was slightly diminished in the KO mice as compared to WT mice. To our surprise, the FDG uptake into iBAT and disappearance of lipid droplets were even more pronounced in *Ucp1* KO mice than in WT mice. This is in stark contrast to the observed defect of *Ucp1* KO mice to reduce iBAT lipid content in response to norepinephrine administration [60]. Thus, in the context of FGFR1/KLB receptor activation, the less energy efficient UCP1-independent thermogenesis may lead to elevated substrate consumption to produce an equivalent amount of heat. Although the nature of this UCP1-independent thermogenesis is still unclear, previous and recent reports suggest the presence of an alternate thermogenic mechanism in brown and beige adipocytes [61–66].

Other metabolic effects such as weight loss and changes in cardiometabolic markers were also observed in *Ucp1* KO mice administered with bFKB1, consistent with previous studies with FGF21. Interestingly, glucose tolerance was improved by bFKB1 in WT mice, but not in *Ucp1* KO mice. In three independent studies with *Ucp1* KO mice, FGF21-induced glucose lowering effects were compromised [31–33]. Therefore, it appears that *Ucp1* is not essential for FGF21- and FGFR1/KLB agonist-induced increase in EE, but is an important contributor to enhanced glucose clearance by these molecules.

The identity of the tissue where the receptor complex that mediates the metabolic effects of FGF21 resides has also been the subject of disagreement. The previous studies utilizing the *aP2*-CRE mediated *Fgfr1* deletion [28,29] were most likely confounded by the non-specific expression of *aP2*-CRE in non-adipocytes such as brain tissue [67], whereas the *Adipoq*-CRE used in this study has been reported to be more adipocyte-selective [45]. Our results with *Adipoq*-CRE mediated *Fgfr1* gene deletion suggest that FGFR1 in adipocytes is indeed essential for the mitogen-activated protein kinase (MAPK) signal activation in adipose tissues by bFKB1, but not for stimulation of BAT thermogenesis or improvement in various markers of metabolic health. Utilizing a newly developed system combining a human FGFR1 selective agonist antibody and tissue-specific transgenic mice, we also demonstrated that BAT-restricted FGFR1 activation is not sufficient to enhance EE, increase *Ucp1* mRNA expression, or alter glucose tolerance. This is in contrast to the action of a non-tissue specific FGFR1 agonist that improves metabolic health independent of appetite control [34]. While this manuscript was in preparation, BonDurant et al. published a study in which they tested the requirement of *Klb* gene in adipocytes in the metabolic action of FGF21 [68]. Their results support our conclusion that FGFR/KLB activation in adipocytes is neither necessary nor sufficient for the chronic metabolic action of FGFR/KLB agonists.

In this study, we demonstrate that bFKB1, like FGF21, decreases preference to saccharin-containing food and ethanol containing water, establishing FGFR1, rather than FGFR2 or FGFR3, as the receptor responsible for aversion to sweet food and alcohol. Our result thus indicates that most of the described activity of FGF21 is mediated by the FGFR1/KLB complex and does not require activation of the FGFR2/KLB or FGFR3/KLB complex. This new observation also suggests a central nervous system-mediated action of bFKB1, despite its large molecular mass (approximately 150 kDa). Human IgG proteins can cross the blood-brain barrier at a very low efficiency [69]. Thus, it is conceivable that a small amount of bFKB1 that crosses the blood-brain barrier may be sufficient to act on a distinct set of FGFR1/KLB-expressing target neurons. Alternatively, bFKB1 may act in the circumventricular organs in the brain that are characterized by extensive vasculature and fenestrated capillaries and thus lack blood brain barrier protection. Further investigation is needed for a more detailed understanding of the FGFR1/KLB expressing neurons. The identification of human FGFR1 selective agonist antibody 14B6 described here should facilitate the functional testing of various neuronal subsets in transgenic mice.

In summary, our study supports a mechanism whereby the FGFR1/KLB agonist antibody bFKB1 stimulates brown fat thermogenesis indirectly through target receptors expressed outside of adipocytes in a manner that does not necessarily require *Ucp1*. Taken together with other available data we believe that molecular-weight-enhanced FGF21-analogs such as Fc-fusions, IgG fusions, and PEGylated FGF21 as well as antibody-based FGF21 mimetics all have a common mechanism of action functioning through the nervous system and more specifically through the FGFR1/KLB complex. The central nervous system is now recognized as the target of various periphery-produced metabolic hormones such as insulin, leptin, and glucagon-like-peptide-1, whose modified forms are used for therapeutic intervention in various metabolic diseases. Additional investigation is warranted to further understand the nature of FGFR1/KLB-expressing neurons and their role in metabolic physiology and the pharmacological action of FGF21-class therapeutics.

AUTHOR CONTRIBUTIONS

M.Z.C. designed and performed experiments, analyzed the data and wrote the manuscript. J.C.C. and J.Z. contributed histological analysis. J.Z-S., L.K., A.O., S.F., V.N., and G.K., designed and performed in vivo studies. M.T., X.B., and K.P. performed in vitro assays. J.C.C., R.N., and S.W. contributed to the generation of *Ucp1-hmFGFR1* transgenic mice. J.S. conceived and supervised the project, performed experiments, analyzed the data and wrote the manuscript.

ACKNOWLEDGEMENTS

We thank Genentech colleagues in Molecular Biology, Antibody Engineering, Protein Chemistry, Biomedical Imaging, Transgenic Technology, Pathology, and Laboratory Animal Resources for technical assistance.

CONFLICT OF INTEREST

All the authors are present or former paid employees of Genentech/Roche.

APPENDIX A. SUPPLEMENTARY DATA

Supplementary data related to this article can be found at http://dx.doi.org/10.1016/j.molmet.2017.09.003.

REFERENCES

[1] Ng, M., Fleming, T., Robinson, M., Thomson, B., Graetz, N., Margono, C., et al., 2014. Global, regional, and national prevalence of overweight and obesity in children and adults during 1980-2013: a systematic analysis for the Global Burden of Disease Study 2013. Lancet 384(9945):766–781.

[2] Deng, T., Lyon, C.J., Bergin, S., Caligiuri, M.A., Hsueh, W.A., 2016. Obesity, Inflammation, and Cancer. Annual Review of Pathology 11:421–449.

[3] Sjöström, L., Narbro, K., Sjöström, C.D., Karason, K., Larsson, B., Wedel, H., et al., 2007. Effects of bariatric surgery on mortality in Swedish obese subjects. The New England Journal of Medicine 357(8):741–752.

[4] Kusminski, C.M., Bickel, P.E., Scherer, P.E., 2016. Targeting adipose tissue in the treatment of obesity-associated diabetes. Nature Review Drug Discovery 15(9):639–660.

[5] Shulman, G.I., 2014. Ectopic fat in insulin resistance, dyslipidemia, and cardiometabolic disease. New England Journal of Medicine 371(12):1131–1141.

[6] Samuel, V.T., Shulman, G.I., 2016. The pathogenesis of insulin resistance: integrating signaling pathways and substrate flux. Journal of Clinical Investigation 126(1):12—22.

[7] Cohen, J.C., Horton, J.D., Hobbs, H.H., 2011. Human fatty liver disease: old questions and new insights. Science 332(6037):1519—1523.

[8] Yoneshiro, T., Aita, S., Matsushita, M., Kayahara, T., Kameya, T., Kawai, Y., et al., 2013. Recruited brown adipose tissue as an antiobesity agent in humans. Journal of Clinical Investigation 123(8):3404—3408.

[9] Nedergaard, J., Cannon, B., 2010. The changed metabolic world with human brown adipose tissue: therapeutic visions. Cell Metabolism 11(4):268—272.

[10] Hany, T.F., Gharehpapagh, E., Kamel, E.M., Buck, A., Himms-Hagen, J., von Schulthess, G.K., 2002. Brown adipose tissue: a factor to consider in symmetrical tracer uptake in the neck and upper chest region. Europian Journal of Nuclear Medicine and Moleluar Imaging 29(10):1393—1398.

[11] Cohade, C., Osman, M., Pannu, H.K., Wahl, R.L., 2003. Uptake in supraclavicular area fat ("USA-Fat"): description on 18F-FDG PET/CT. Journal of Nuclear Medicine 44(2):170—176.

[12] Cypess, A.M., Kahn, C.R., 2010. Brown fat as a therapy for obesity and diabetes. Current Opinion in Endocrinology, Diabetes and Obesity 17(2):143—149.

[13] Cannon, B., Nedergaard, J., 2004. Brown adipose tissue: function and physiological significance. Physiological Reviews 84(1):277—359.

[14] Bertholet, A.M., Kirichok, Y., 2017. UCP1: a transporter for H+ and fatty acid anions. Biochimie 134:28—34.

[15] Yoneshiro, T., Aita, S., Matsushita, M., Kameya, T., Nakada, K., Kawai, Y., et al., 2011. Brown adipose tissue, whole-body energy expenditure, and thermogenesis in healthy adult men. Obesity 19(1):13—16.

[16] Walden, T.B., Hansen, I.R., Timmons, J.A., Cannon, B., Nedergaard, J., 2012. Recruited vs. nonrecruited molecular signatures of brown, "brite," and white adipose tissues. American Journal of Physiology — Endocrinology and Metabolism 302(1):E19—E31.

[17] Owen, B.M., Mangelsdorf, D.J., Kliewer, S.A., 2015. Tissue-specific actions of the metabolic hormones FGF15/19 and FGF21. Trends in Endocrinology and Metabolism 26(1):22—29.

[18] Kharitonenkov, A., DiMarchi, R., 2015. FGF21 revolutions: recent advances illuminating FGF21 Biology and medicinal properties. Trends in Endocrinology and Metabolism 26(11):608—617.

[19] Xu, J., Lloyd, D.J., Hale, C., Stanislaus, S., Chen, M., Sivits, G., et al., 2009. Fibroblast growth factor 21 reverses hepatic steatosis, increases energy expenditure, and improves insulin sensitivity in diet-induced obese mice. Diabetes 58(1):250—259.

[20] Coskun, T., Bina, H.A., Schneider, M.A., Dunbar, J.D., Hu, C.C., Chen, Y., et al., 2008. Fibroblast growth factor 21 corrects obesity in mice. Endocrinology 149(12):6018—6027.

[21] Gaich, G., Chien, J.Y., Fu, H., Glass, L.C., Deeg, M.A., Holland, W.L., et al., 2013. The effects of LY2405319, an FGF21 analog, in obese human subjects with type 2 diabetes. Cell Metabolism 18(3):333—340.

[22] Kharitonenkov, A., Wroblewski, V.J., Koester, A., Chen, Y.-F., Clutinger, C.K., Tigno, X.T., et al., 2007. The metabolic state of diabetic monkeys is regulated by fibroblast growth factor-21. Endocrinology 148(2):774—781.

[23] Adams, A.C., Halstead, C.A., Hansen, B.C., Irizarry, A.R., Martin, J.A., Myers, S.R., et al., 2013. LY2405319, an engineered FGF21 variant, improves the metabolic status of diabetic monkeys. PLoS One 8(6):e65763.

[24] Talukdar, S., Zhou, Y., Li, D., Rossulek, M., Dong, J., Somayaji, V., et al., 2016. A long-acting FGF21 molecule, PF-05231023, decreases body weight and improves lipid profile in non-human primates and type 2 diabetic subjects. Cell Metabolism 23(3):427—440.

[25] Veniant, M.M., Komorowski, R., Chen, P., Stanislaus, S., Winters, K., Hager, T., et al., 2012. Long-acting FGF21 has enhanced efficacy in diet-induced obese mice and in obese rhesus monkeys. Endocrinology 153(9):4192—4203.

[26] Ogawa, Y., Kurosu, H., Yamamoto, M., Nandi, A., Rosenblatt, K.P., Goetz, R., et al., 2007. BetaKlotho is required for metabolic activity of fibroblast growth factor 21. Proceedings of the National Academy of Sciences of the United States of America 104(18):7432—7437.

[27] Kurosu, H., Choi, M., Ogawa, Y., Dickson, A.S., Goetz, R., Eliseenkova, A.V., et al., 2007. Tissue-specific expression of betaKlotho and fibroblast growth factor (FGF) receptor isoforms determines metabolic activity of FGF19 and FGF21. Journal of Biological Chemistry 282(37):26687—26695.

[28] Adams, A.C., Yang, C., Coskun, T., Cheng, C.C., Gimeno, R.E., Luo, Y., et al., 2012. The breadth of FGF21's metabolic actions are governed by FGFR1 in adipose tissue. Moleular Metabolism 2(1):31—37.

[29] Foltz, I.N., Hu, S., King, C., Wu, X., Yang, C., Wang, W., et al., 2012. Treating diabetes and obesity with an FGF21-mimetic antibody activating the beta-Klotho/FGFR1c receptor complex. Science Translational Medicine 4(162), 162ra53.

[30] Kolumam, G., Chen, M.Z., Tong, R., Zavala-Solorio, J., Kates, L., van Bruggen, N., et al., 2015. Sustained brown fat stimulation and insulin sensitization by a humanized bispecific antibody agonist for fibroblast growth factor receptor 1/betaKlotho complex. EBioMedicine 2(7):730—743.

[31] Samms, R.J., Smith, D.P., Cheng, C.C., Antonellis, P.P., Perfield 2nd, J.W., Kharitonenkov, A., et al., 2015. Discrete aspects of FGF21 in vivo pharmacology do not require UCP1. Cell Report 11(7):991—999.

[32] Veniant, M.M., Sivits, G., Helmering, J., Komorowski, R., Lee, J., Fan, W., et al., 2015. Pharmacologic effects of FGF21 are independent of the "browning" of white adipose tissue. Cell Metabolism 21(5):731—738.

[33] Kwon, M.M., O'Dwyer, S.M., Baker, R.K., Covey, S.D., Kieffer, T.J., 2015. FGF21-Mediated improvements in glucose clearance require uncoupling protein 1. Cell Report 13(8):1521—1527.

[34] Wu, A.L., Kolumam, G., Stawicki, S., Chen, Y., Li, J., Zavala-Solorio, J., et al., 2011. Amelioration of type 2 diabetes by antibody-mediated activation of fibroblast growth factor receptor 1. Science Translational Medicine 3(113), 113ra26.

[35] Véniant, M.M., Hale, C., Helmering, J., Chen, M.M., Stanislaus, S., Busby, J., et al., 2012. FGF21 promotes metabolic homeostasis via white adipose and leptin in mice. PLoS One 7(7):e40164.

[36] Ding, X., Boney-Montoya, J., Owen, B.M., Bookout, A.L., Coate, K.C., Mangelsdorf, D.J., et al., 2012. Betaklotho is required for fibroblast growth factor 21 effects on growth and metabolism. Cell Metabolism 16(3):387—393.

[37] Fon Tacer, K., Bookout, A.L., Ding, X., Kurosu, H., John, G.B., Wang, L., et al., 2010. Research resource: comprehensive expression atlas of the fibroblast growth factor system in adult mouse. Molecular Endocrinology 24(10):2050—2064.

[38] Fisher, F.M., Kleiner, S., Douris, N., Fox, E.C., Mepani, R.J., Verdeguer, F., et al., 2012. FGF21 regulates PGC-1α and browning of white adipose tissues in adaptive thermogenesis. Genes and Development 26(3):271—281.

[39] Bookout, A.L., de Groot, M.H., Owen, B.M., Lee, S., Gautron, L., Lawrence, H.L., et al., 2013. FGF21 regulates metabolism and circadian behavior by acting on the nervous system. Nature Medicine 19(9):1147—1152.

[40] Owen, B.M., Ding, X., Morgan, D.A., Coate, K.C., Bookout, A.L., Rahmouni, K., et al., 2014. FGF21 acts centrally to induce sympathetic nerve activity, energy expenditure, and weight loss. Cell Metabolism 20(4):670—677.

[41] Lo, M., Kim, H.S., Tong, R.K., Bainbridge, T.W., Vernes, J.M., Zhang, Y., et al., 2017. Effector-attenuating substitutions that maintain antibody stability and reduce toxicity in mice. Journal of Biological Chemistry 292(9):3900—3908.

[42] Enerback, S., Jacobsson, A., Simpson, E.M., Guerra, C., Yamashita, H., Harper, M.E., et al., 1997. Mice lacking mitochondrial uncoupling protein are cold-sensitive but not obese. Nature 387(6628):90—94.

[43] Hoch, R.V., Soriano, P., 2006. Context-specific requirements for Fgfr1 signaling through Frs2 and Frs3 during mouse development. Development 133(4):663—673.

[44] Eguchi, J., Wang, X., Yu, S., Kershaw, E.E., Chiu, P.C., Dushay, J., et al., 2011. Transcriptional control of adipose lipid handling by IRF4. Cell Metabolism 13(3):249—259.

[45] Jeffery, E., Berry, R., Church, C.D., Yu, S., Shook, B.A., Horsley, V., et al., 2014. Characterization of Cre recombinase models for the study of adipose tissue. Adipocyte 3(3):206–211.

[46] Guerra, C., Navarro, P., Valverde, A.M., Arribas, M., Bruning, J., Kozak, L.P., et al., 2001. Brown adipose tissue-specific insulin receptor knockout shows diabetic phenotype without insulin resistance. Journal of Clinical Investigation 108(8):1205–1213.

[47] Cirera, S., 2013. Highly efficient method for isolation of total RNA from adipose tissue. BMC Research Notes 6:472.

[48] Feldmann, H.M., Golozoubova, V., Cannon, B., Nedergaard, J., 2009. UCP1 ablation induces obesity and abolishes diet-induced thermogenesis in mice exempt from thermal stress by living at thermoneutrality. Cell Metabolism 9(2):203–209.

[49] Kazak, L., Chouchani, E.T., Stavrovskaya, I.G., Lu, G.Z., Jedrychowski, M.P., Egan, D.F., et al., 2017. UCP1 deficiency causes brown fat respiratory chain depletion and sensitizes mitochondria to calcium overload-induced dysfunction. Proceedings of the National Academy of Sciences of the United States of America 114(30):7981–7986.

[50] Bernardo, B., Lu, M., Bandyopadhyay, G., Li, P., Zhou, Y., Huang, J., et al., 2015. FGF21 does not require interscapular brown adipose tissue and improves liver metabolic profile in animal models of obesity and insulin-resistance. Scientific Reports 5:11382.

[51] Ornitz, D.M., Itoh, N., 2015. The fibroblast growth factor signaling pathway. Wiley interdisciplinary reviews. Developmental Biology 4(3):215–266.

[52] Muise, E.S., Souza, S., Chi, A., Tan, Y., Zhao, X., Liu, F., et al., 2013. Downstream signaling pathways in mouse adipose tissues following acute in vivo administration of fibroblast growth factor 21. PLoS One 8(9):e73011.

[53] Yu, P., Wilhelm, K., Dubrac, A., Tung, J.K., Alves, T.C., Fang, J.S., et al., 2017. FGF-dependent metabolic control of vascular development. Nature 545(7653):224–228.

[54] Patel, N.G., Kumar, S., Eggo, M.C., 2005. Essential role of fibroblast growth factor signaling in preadipoctye differentiation. Journal of Clinical Endocrinology and Metabolism 90(2):1226–1232.

[55] Brogi, E., Winkles, J.A., Underwood, R., Clinton, S.K., Alberts, G.F., Libby, P., 1993. Distinct patterns of expression of fibroblast growth factors and their receptors in human atheroma and nonatherosclerotic arteries. Association of acidic FGF with plaque microvessels and macrophages. Journal of Clinical Investigation 92(5):2408–2418.

[56] Talukdar, S., Owen, B.M., Song, P., Hernandez, G., Zhang, Y., Zhou, Y., et al., 2016. FGF21 regulates sweet and alcohol preference. Cell Metabolism 23(2):344–349.

[57] von Holstein-Rathlou, S., BonDurant, L.D., Peltekian, L., Naber, M.C., Yin, T.C., Claflin, K.E., et al., 2016. FGF21 mediates endocrine control of simple sugar intake and sweet taste preference by the liver. Cell Metabolism 23(2):335–343.

[58] Sonoda, J., Chen, M.Z., Baruch, A., 2017. FGF21-receptor agonists: an emerging therapeutic class for obesity-related diseases. Hormone Molecular Biology and Clinical Investigation 30(2).

[59] Golozoubova, V., Hohtola, E., Matthias, A., Jacobsson, A., Cannon, B., Nedergaard, J., 2001. Only UCP1 can mediate adaptive nonshivering thermogenesis in the cold. FASEB Journal 15(11):2048–2050.

[60] Grimpo, K., Volker, M.N., Heppe, E.N., Braun, S., Heverhagen, J.T., Heldmaier, G., 2014. Brown adipose tissue dynamics in wild-type and UCP1-knockout mice: in vivo insights with magnetic resonance. Journal of Lipid Research 55(3):398–409.

[61] Bal, N.C., Maurya, S.K., Sopariwala, D.H., Sahoo, S.K., Gupta, S.C., Shaikh, S.A., et al., 2012. Sarcolipin is a newly identified regulator of muscle-based thermogenesis in mammals. Nature Medicine 18(10):1575–1579.

[62] Ukropec, J., Anunciado, R.P., Ravussin, Y., Hulver, M.W., Kozak, L.P., 2006. UCP1-independent thermogenesis in white adipose tissue of cold-acclimated Ucp1-/- mice. Journal of Biological Chemistry 281(42):31894–31908.

[63] Kazak, L., Chouchani, E.T., Jedrychowski, M.P., Erickson, B.K., Shinoda, K., Cohen, P., et al., 2015. A creatine-driven substrate cycle enhances energy expenditure and thermogenesis in beige fat. Cell. 163(3):643–655.

[64] Long, J.Z., Svensson, K.J., Bateman, L.A., Lin, H., Kamenecka, T., Lokurkar, I.A., et al., 2016. The secreted enzyme PM20D1 regulates lipidated amino acid uncouplers of mitochondria. Cell. 166(2):424–435.

[65] Bertholet, A.M., Kazak, L., Chouchani, E.T., Bogaczynska, M.G., Paranjpe, I., Wainwright, G.L., et al., 2017. Mitochondrial patch clamp of beige adipocytes reveals UCP1-positive and UCP1-negative cells both exhibiting futile creatine cycling. Cell Metabolism 25(4):811–822.

[66] Caron, A., Labbe, S.M., Carter, S., Roy, M.C., Lecomte, R., Ricquier, D., et al., 2017. Loss of UCP2 impairs cold-induced non-shivering thermogenesis by promoting a shift toward glucose utilization in brown adipose tissue. Biochimie 134:118–126.

[67] Martens, K., Bottelbergs, A., Baes, M., 2010. Ectopic recombination in the central and peripheral nervous system by aP2/FABP4-Cre mice: implications for metabolism research. FEBS Letters 584(5):1054–1058.

[68] BonDurant, L.D., Ameka, M., Naber, M.C., Markan, K.R., Idiga, S.O., Acevedo, M.R., et al., 2017. FGF21 regulates metabolism through adipose-dependent and -independent mechanisms. Cell Metabolism 25(4):935–944.

[69] Yu, Y.J., Zhang, Y., Kenrick, M., Hoyte, K., Luk, W., Lu, Y., et al., 2011. Boosting brain uptake of a therapeutic antibody by reducing its affinity for a transcytosis target. Science Translational Medicine 3(84), 84ra44.

